doi:10.1016/j.jmb.2011.06.030 J. Mol. Biol. (2011) 411, 765–780

Contents lists available at www.sciencedirect.com

Journal of Molecular Biology

journal homepage: http://ees.elsevier.com.jmb

Multiple Factors Insulate Msh2–Msh6 Mismatch Repair Activity from Defects in Msh2 Domain I

Charanya Kumar[1]†, Sarah C. Piacente[1]†, Justin Sibert[2], Andrew R. Bukata[1], Jaime O'Connor[1], Eric Alani[2] and Jennifer A. Surtees[1]*

[1]*Department of Biochemistry, School of Medical and Biomedical Sciences, State University of New York at Buffalo, Buffalo, NY 14214, USA*
[2]*Department of Molecular Biology and Genetics, Cornell University, Ithaca, NY 14853-2703, USA*

Received 15 February 2011; received in revised form 13 June 2011; accepted 14 June 2011
Available online 25 June 2011

Edited by M. Gottesman

Keywords:
mismatch repair; Msh2–Msh6; mutator phenotype; hereditary non-polyposis colorectal cancer; *Saccharomyces cerevisiae*

DNA mismatch repair (MMR) is a highly conserved mutation avoidance mechanism that corrects DNA polymerase misincorporation errors. In initial steps in MMR, Msh2–Msh6 binds mispairs and small insertion/deletion loops, and Msh2–Msh3 binds larger insertion/deletion loops. The *msh2Δ1* mutation, which deletes the conserved DNA-binding domain I of Msh2, does not dramatically affect Msh2–Msh6-dependent repair. In contrast, *msh2Δ1* mutants show strong defects in Msh2–Msh3 functions. Interestingly, several mutations identified in patients with hereditary non-polyposis colorectal cancer map to domain I of Msh2; none have been found in *MSH3*. To understand the role of Msh2 domain I in MMR, we examined the consequences of combining the *msh2Δ1* mutation with mutations in two distinct regions of *MSH6* and those that increase cellular mutational load (*pol3-01* and *rad27*). These experiments reveal *msh2Δ1*-specific phenotypes in Msh2–Msh6 repair, with significant effects on mutation rates. *In vitro* assays demonstrate that msh2Δ1–Msh6 DNA binding is less specific for DNA mismatches and produces an altered footprint on a mismatch DNA substrate. Together, these results provide evidence that, *in vivo*, multiple factors insulate MMR from defects in domain I of Msh2 and provide insights into how mutations in Msh2 domain I may cause hereditary non-polyposis colorectal cancer.

Introduction

DNA mismatch repair (MMR) systems promote genome stability by correcting nucleotide incorporation errors that occur at the replication fork, by regulating genetic recombination and by signaling cellular responses to DNA damage.[1–3] In each case, the first step in initiating a DNA repair response is recognizing the presence of a lesion. This task is performed by the MutS family proteins: MutS in prokaryotic cells and MutS homologs (Msh) in eukaryotic cells. In eukaryotic MMR, two heterodimeric Msh complexes recognize and bind a mispair: Msh2–Msh6 and Msh2–Msh3. Once the

*Corresponding author. E-mail address: jsurtees@buffalo.edu.

† C.K. and S.C.P. contributed equally to this work.

Abbreviations used: MMR, mismatch repair; HNPCC, hereditary non-polyposis colorectal cancer; IDL, insertion/deletion loop; PIP, PCNA interaction peptide; NTR, N-terminal region; SEM, standard error of the mean; EDTA, ethylenediaminetetraacetic acid; OP-Cu, 1,10-phenanthroline–copper; PCNA, proliferating cell nuclear antigen; SC, synthetic complete.

lesion has been recognized, MutL homolog (Mlh) proteins are recruited in an ATP-dependent manner to form a ternary complex. The ternary complex initiates downstream events, including unwinding of the DNA and excision of the nascent strand. This is followed by DNA resynthesis and ligation to fill the resulting gap. ATP binding and hydrolysis by Msh and Mlh complexes are essential for downstream events. The mutation rate increases 100- to 1000-fold when MMR is inactivated.[1,4] The importance of effective MMR in maintaining genome stability is emphasized by the fact that defects in human MMR are associated with hereditary nonpolyposis colorectal cancer (HNPCC), a dominant cancer syndrome that results in early age of disease onset and increased susceptibility to a number of cancers. HNPCC-associated mutations in MMR are primarily in *MSH2* (~40%), *MSH6* (~10%) and *MLH1* (~50%).[5] None has been identified in *MSH3*, although several studies have screened for such mutations.[6] Recently, one study has identified *MSH3* alleles that are associated with HNPCC, but only in combination with alleles in *MSH2*.[7]

The Msh complexes, Msh2–Msh3 and Msh2–Msh6, have distinct yet overlapping specificities in mismatch recognition. Msh2–Msh6 recognizes and binds mispairs and small insertion/deletion loops (IDLs) of one to two nucleotides. Msh2–Msh3 is primarily responsible for binding larger IDLs, including loops of up to 17 nucleotides in length,[8] although Msh2–Msh3 has also been shown to bind some mispairs.[9] We were intrigued by the contribution of Msh2 to the DNA lesion recognition and binding properties of each complex. We have focused on domain I of Msh2, one of two putative DNA-binding domains in the protein. Fourteen mutations in this region have been identified in HNPCC patients (Fig. 1),[10,11–16] several of which have been shown to have at least a mild effect on MMR activity.[17,18] Recently, deletions of Msh2

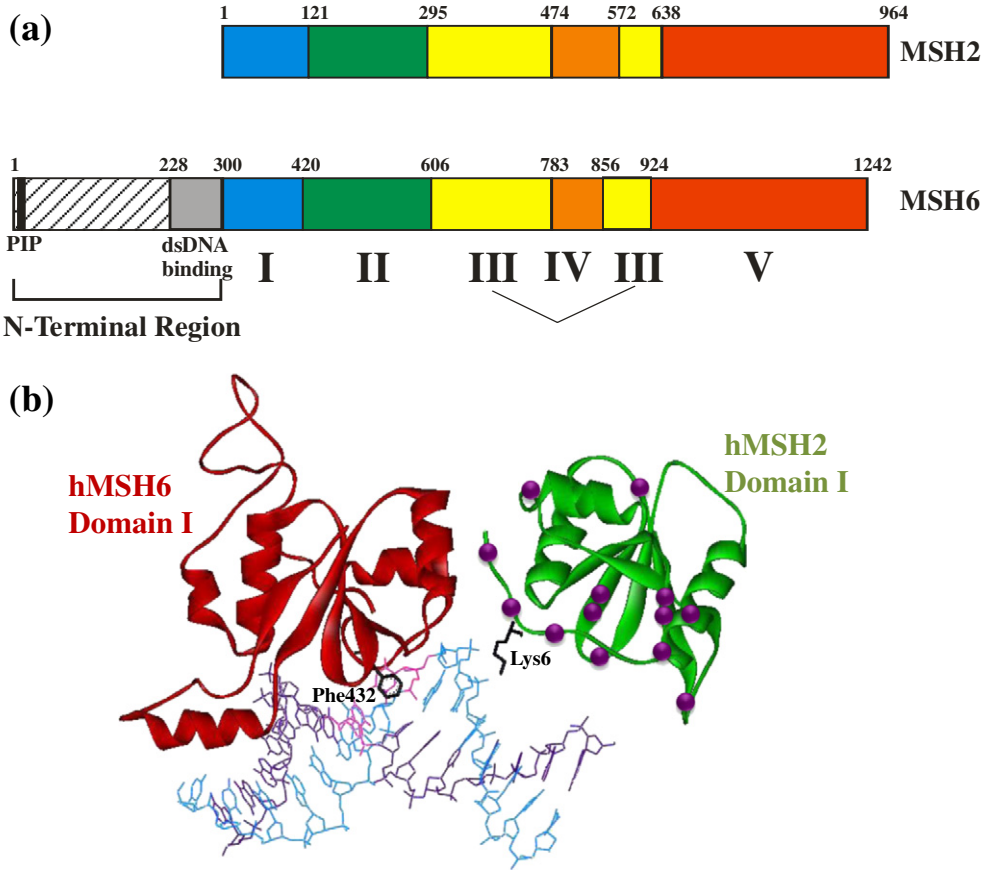

Fig. 1. (a) Schematic of the domain structure of Msh2 and Msh6 based on homology with the human proteins.[10] Domains I–V are defined by the MutS and MutSα crystal structures.[10,22] The NTR is defined based on Clark *et al.*[40] (b) Structure of domain I of hMSH2 (green) and hMSH6 (red) with locations of HNPCC mutations in hMSH2 domain I indicated by the purple spheres. Lysine 6 of hMSH2 and the mispair-binding phenylalanine 432 of hMSH6 are shown in black. The DNA mispair is colored pink. This figure was generated in WebLab Viewer using data from Warren *et al.*[10]

domain I have also been identified in HNPCC patients.[19,20] However, the role of this domain in maintaining genome stability is not clear.

The crystal structures of MutS from *Escherichia coli* and *Thermus aquaticus* indicated that each MutS subunit folds into five distinct domains (Fig. 1a).[21,22] Domains I and IV interact with DNA, with residues in domain I making specific contacts with the mispair through a conserved Phe-X-Glu motif.[21–23] Despite being composed of two identical subunits, the MutS complex interacts asymmetrically with the mispair. Only one subunit makes specific contacts with the mispair, while domain I of the non-mismatch binding MutS subunit makes substantial nonspecific contacts with the phosphodiester backbone.

In the eukaryotic heterodimeric complexes, the domain structure is conserved (Fig. 1a), and Msh2 appears to be the non-mismatch binding subunit. Domain I of Msh2 does not encode the conserved mispair recognition motif (F-X-E) required for Msh2–Msh6 interactions with a mispair,[24–27] and Msh2 domain I is not required for specific interactions between Msh2–Msh3 and its loop substrates.[28,29] In contrast to the prokaryotic systems, the crystal structure of human MutSα (Msh2–Msh6) indicates that Msh2 domain I makes only one contact with the DNA through a lysine residue (Fig. 1b).[10] In fact, the 14 N-terminal residues form an extended strand that blocks Msh2 DNA binding.

Previously, we deleted the entirety of Msh2 domain I (referred to as *msh2Δ1*), based on the *Taq* MutS crystal structure,[22] and characterized the effect of this mutation with respect to Msh2–Msh3 and Msh2–Msh6 functions in *Saccharomyces cerevisiae*.[28,30] We found that, *in vivo*, *msh2Δ1* was a separation-of-function mutation: Msh2–Msh6 function was largely unaffected, while Msh2–Msh3 function was completely abolished.[28,30]

In vitro, msh2Δ1–Msh3 was severely impaired for its overall DNA-binding activity, indicating a much reduced affinity for DNA.[28] Despite this, 1,10-phenanthroline–copper (OP-Cu) footprinting studies demonstrated similar patterns of protection of a +8 loop substrate in the presence of msh2Δ1–Msh3 and Msh2–Msh3, indicating that the deleted form of the protein forms a nucleoprotein complex similar to that formed by the wild-type Msh2–Msh3 complex. We concluded that Msh2 domain I makes nonspecific contacts that are important for Msh2–Msh3 to interact with the DNA substrate, but not in forming a distinct and specific protein–DNA conformation. The severely reduced affinity of msh2Δ1–Msh3 for DNA presumably accounts for a significant portion of the strong Msh2–Msh3-specific defect *in vivo* in the presence of the *msh2Δ1* allele.[28]

In contrast to Msh2–Msh3, Msh2–Msh6 function *in vivo* was largely unaffected by the presence of the *msh2Δ1* mutation, indicating that Msh2 domain I plays a distinct role in Msh2–Msh3 *versus* Msh2–Msh6 activity in yeast. Furthermore, it appeared that Msh2 domain I is dispensable for Msh2–Msh6 function. An alternative possibility is that the very mild phenotype is a result of additional factors *in vivo* that compensate for any biochemical defects in the msh2Δ1–Msh6 complex, thereby buffering the MMR system from these defects. As shown below, we found that domain I of Msh2 is required for wild-type DNA-binding activity of Msh2–Msh6 *in vitro*. However, this defect is masked *in vivo* by a number of factors/conditions, including mutational load, interactions with the DNA polymerase processivity factor proliferating cell nuclear antigen (PCNA) and the N-terminal region (NTR) of Msh6. Our observations demonstrate the robustness of MMR and, particularly, Msh2–Msh6-specific MMR *in vivo*.

Results

msh2Δ1 has subtle effects on Msh2–Msh6 function *in vivo*

The *msh2Δ1* allele results in the deletion of residues 2–133 of Msh2. Despite this substantial alteration in the coding sequence, previous work has indicated that Msh2–Msh6-specific functions were largely unaffected in *msh2Δ1* mutants (Table 1).[28,30] We created the *msh2Δ1* allele in a strain background (FY23 and FY86)[31] without the hemagglutinin tag that was present in our earlier work (see Materials and Methods; Table S1). In this study, we were interested in specifically looking at Msh2–Msh6

Table 1. *CAN1* mutation rates in *msh2Δ1* mutants

Genotype	Can^R rate ($\times 10^{-7}$)	Relative to wild type
Wild type	1.8 (1.4–2.2)[a]	1.0
msh2Δ1	2.7 (2.3–3.1)	1.5
msh3Δ	3.0 (2.2–3.9)	1.7
msh6Δ	25.4 (22.3–28.7)	14.1
msh2Δ	48.8 (43.9–53.9)	27.1
pol3-01	77.2 (69.3–85.4)	42.9
rad27G67S	18.4 (15.7–21.3)	10.2
msh6KQFF→AAAA	4.4 (3.0–5.9)	2.4
msh2Δ1 pol3-01	229.2 (218.7–240.0)	127.3
msh2Δ1 rad27G67S	28.9 (26.8–31.1)	16.1
msh2Δ1 msh3Δ	4.4 (3.5–5.4)	2.4
msh2Δ1 msh6KQFF→AAAA	5.7 (4.9–6.5)	3.2
msh3Δ msh6KQFF→AAAA	4.8 (4.0–5.7)	2.7
msh2Δ1 msh3Δ msh6KQFF→AAAA	11.8 (10.4–13.2)	6.6

[a] Canavanine assays were performed as described in Materials and Methods. Strains used in these studies are shown in Table S1. The 95% confidence intervals are in parentheses.

function *in vivo*. For this reason, we chose to use the canavanine resistance assay to measure mutation rates. This assay identifies primarily −1 frameshifts and base substitutions in *CAN1* (the preferred substrates for Msh2–Msh6) that lead to resistant colonies; *msh3Δ* has only a very weak phenotype in this assay (Table 1).[9,30,32,33] There was a small but statistically significant increase in *CAN1* mutation rates in the *msh2Δ1* strains constructed for this study relative to the *MSH2* controls, similar to previous observations.[30] The mutation rate in the *msh2Δ1* background was comparable to that in the *msh3Δ* background (1.5-fold *versus* 1.7-fold increase over wild type, respectively). In contrast, an *msh6Δ* resulted in a 14-fold increase in mutation rate over wild type, similar to previous observations.[30,33] This is consistent with *msh2Δ1* conferring an Msh2–Msh3-specific phenotype.

To test for subtle MMR defects in *msh2Δ1*, we performed mutation spectrum analysis by sequencing the *CAN1* gene in canavanine-resistant papillations (Table 2). We found that the mutation spectrum in *msh2Δ1* was distinct from that in *msh3Δ*.[9] In *msh2Δ1*, the frequency of frameshift mutations was 31%, similar to the observed 34% frequency in *msh3Δ* and consistent with a defect in Msh2–Msh3 activity.[9] However, the frequency of base substitutions in *msh2Δ1* (60%) was intermediate to that observed in *msh3Δ* (46%)[9] and in *msh6Δ* (86–89%)[9,33] and is similar to the observed frequency in *msh3Δ msh6Δ* (68%),[33] indicating a possible defect in both Msh2–Msh3 and Msh2–Msh6 functions.

Increasing cellular mutational load has a significant effect on mutation rate in *msh2Δ1* background

The mutation spectra seen in *msh2Δ1* strains suggest subtle defects in msh2Δ1–Msh6 function. We reasoned that a defect in msh2Δ1–Msh6 function might be masked by the high fidelity (mutation rates: 1×10^{-6} to 1×10^{-7})[34] of the replicative polymerases. If the mutation rate is low, then the requirement for MMR would be similarly low. To test this, we combined the *msh2Δ1* allele with mutations that increase the mutational load of the cell. First, we introduced an allele of *rad27*, *rad27G67S*,[35] into the *msh2Δ1* background. This allele causes an increase in mutation rate by affecting the nuclease functions of Rad27, a flap endonuclease that acts in Okazaki fragment processing. The *rad27G67S* allele had a 10.2-fold increase in mutation rate over the wild type in the canavanine resistance assay. When combined with *msh2Δ1*, this allele conferred a mutation rate 16-fold above wild type (Table 1). This is a multiplicative effect of the two mutations, indicating a defect in both pathways; however, the result is somewhat subtle. To test a higher background mutation rate, we next introduced the *pol3-01* allele into the *msh2Δ1* background. *pol3-01* encodes a mutation in the exonuclease function of polymerase δ[36,37] and increases the mutation rate in the cell 43-fold over wild type. *pol3-01 msh2Δ1* mutants showed a 127-fold increase in mutation rate over the wild type (Table 1), a greater than multiplicative effect on mutation rate. Thus, there is a synergistic effect between these mutations that increase the cells' mutational load and *msh2Δ1*, suggesting that *msh2Δ1* may cripple MMR in a manner that becomes functionally relevant in the presence of a higher background mutation rate.

Table 2. *CAN1* locus mutation spectrum

Genotype (strain)	Percent of each mutation type			
	Base substitution	Frameshift	Other[a]	*n*[b]
Wild type (EAY236)	76	17	7	29
msh2Δ1 (EAY2039 and EAY2040)	60	31	9	68

The *CAN1* locus was PCR amplified and sequenced from canavanine-resistant colonies obtained from wild-type and *msh2Δ1* strains.
[a] Refers to larger deletion, insertion or recombination events.
[b] Number of mutations identified in *CAN1*.

An interaction with PCNA facilitates msh2Δ1–Msh6-directed repair

Our analysis of *msh2Δ1* in *pol3-01* and *rad27* strains suggested that additional DNA repair factors buffer *msh2Δ1* defects. We tested whether PCNA interactions could mask defects in Msh2 function through its interaction with Msh6. Msh2–Msh6 interacts with DNA polymerase processivity factor PCNA through a conserved consensus PCNA interaction peptide (PIP) box near the N-terminus of Msh6.[38,39] This interaction has been suggested to recruit or retain MMR proteins to the replisome. Disruption of this motif impairs Msh6 interactions with PCNA and leads to a small increase (~2-fold) in mutation rate *in vivo*, as measured in the canavanine assay.[38,39] We reasoned that an interaction with PCNA might localize msh2Δ1–Msh6 to the replication fork, where it would be in close proximity to nascent mispairs. This would create a high local concentration of msh2Δ1–Msh6 that might compensate for the *in vitro* defects in substrate affinity that we observed (see below). To test this, we introduced chromosomal mutations in *MSH6*, replacing the KQFF consensus residues with AAAA.[38] As previously observed, the mutation in the PIP box alone resulted in a 2.4-fold increase in mutation rate (Table 1), similar to that observed in an *msh2Δ1* or an *msh3Δ* background, which,

although small, was statistically significant. When this allele was combined with *msh3Δ* or with *msh2Δ1*, there was a 2.7- or 3.2-fold increase in mutation rate over the wild type, respectively (Table 1),[38,39] which was statistically significant ($p<0.001$). In the *msh2Δ1 msh3Δ msh6AAAA* background, we observed a 6.6-fold increase in mutation rate over wild type (Table 1). This is a significant increase, indicating that the PIP box motif in Msh6 helps buffer the effects of the deletion of Msh2 domain I *in vivo*. Furthermore, the fact that the triple mutant has a mutation rate that is higher than that of either double mutant indicates that Msh2 domain I plays a role outside of Msh2–Msh3 function, perhaps aiding in interactions with PCNA.

Additional portions of *MSH6* NTR buffer *msh2Δ1* defects in MMR

The PIP box motif is located at the extreme of the so-called NTR of Msh6. This region is upstream of Msh6 domain I and is not present in MutS or Msh2 proteins. Recently, an additional functional domain within the NTR was identified and was demonstrated to have nonspecific duplex DNA-binding activity *in vitro*.[40] Disruption of this nonspecific DNA-binding region (residues 228–299 in yeast Msh6), by deletion or substitution, reduced DNA binding *in vitro* and caused modest increases in mutation rates *in vivo*,[40] indicating that it has a role in Msh2–Msh6 function.

We examined the effect of four mutations in the NTR DNA-binding region, *msh6Δ252–299*, *msh6Δ269–299*, *msh6Δ290–299* and *msh6 K232E K271E R289E*, on mutation rates in the presence of *msh2Δ1*. In each strain background, a low-copy (*ARS-CEN*) plasmid carrying an empty vector, wild-type *MSH6* or one of four *msh6* alleles was introduced into an *msh6Δ* background. As previously described,[40] the deletion alleles *msh6Δ252–299*, *msh6Δ269–299* and *msh6Δ290–299* resulted in small but significant ($p<0.001$) increases in mutation rate (Table 3), approximately 2.3- to 3.3-fold over the wild-type background, in the canavanine resistance assay. This is similar to the effect of the *msh2Δ1* allele. However, when these *msh6* alleles were present in an *msh2Δ1* background, there were synergistic increases in mutation rate, ranging from 11.7- to 18.8-fold over wild type. This phenotype was not simply a result of the loss of Msh2–Msh3 function in an *msh2Δ1* background.[28] In an *msh3Δ* background, there was an increase in mutation rate in the presence of the *msh6* alleles but only an approximately 2- to 3-fold increase over the *msh6* alleles on their own, roughly half or less of the effect observed with the *msh2Δ1* allele. Furthermore, in the *msh3Δ msh2Δ1* background, the *msh6* alleles led to even higher mutation rates, with a roughly additive effect. This indicates that defects in both Msh2–Msh3 and Msh2–Msh6 functions are contributing to the elevated mutation rate.

Table 3. *CAN1* mutation rates in the presence of *msh6* NTR alleles expressed on *ARS-CEN* vectors

Relevant genotype (strain)	Can^R rate ($\times 10^{-7}$)	Relative to wild type
MSH6[a]	2.1 (1.6–2.7)[b]	1.0
msh2Δ1[a]	5.4 (4.5–6.4)	2.5
msh3Δ[a]	4.8 (3.6–6.1)	2.3
msh2Δ1 msh3Δ[a]	8.9 (7.3–10.7)	4.2
msh6Δ[c]	19.2 (17.0–21.4)	9.0
msh2Δ1 msh6Δ[c]	55.6 (52.3–59.0)	26.1
msh3Δ msh6Δ[c]	33.0 (28.5–37.7)	15.5
msh2Δ1msh3Δ msh6Δ[c]	67.8 (61.9–73.8)	31.8
msh6-R232E K271E R289[d]	2.8 (2.1–3.6)	1.3
msh2Δ1 msh6-R232E K271E R289E[d]	10.0 (8.8–11.4)	4.7
msh3Δ msh6-R232E K271E R289E[d]	8.1 (6.3–10.2)	3.8
msh2Δ1 msh3Δ msh6-R232E K271E R289E[d]	26.2 (22.3–30.4)	12.3
msh6Δ290–299[e]	4.9 (4.0–5.9)	2.3
msh2Δ1 msh6Δ290–299[e]	25.0 (22.5–27.6)	11.7
msh3Δ msh6Δ290–299[e]	13.9 (11.2–16.8)	6.5
msh2Δ1 msh3Δ msh6Δ290–299[e]	41.3 (36.7–46.1)	19.4
msh6Δ269–299[f]	6.1 (4.9–7.3)	2.9
msh2Δ1 msh6Δ269–299[f]	40.0 (36.8–43.4)	18.8
msh3Δ msh6Δ269–299[f]	14.6 (12.0–17.4)	6.9
msh2Δ1 msh3Δ msh6Δ269–299[f]	44.7 (38.5–51.2)	21.0
msh6Δ252–299[g]	7.1 (6.0–8.2)	3.3
msh2Δ1 msh6Δ252–299[g]	35.9 (32.1–39.9)	16.9
msh3Δ msh6Δ252–299[g]	17.4 (14.4–20.7)	8.2
msh2Δ1 msh3Δ msh6Δ252–299[g]	62.7 (54.5–71.4)	29.5

[a] *msh6Δ* strains transformed with pCK1 encoding *MSH6*.
[b] Canavanine assays were performed as described in Materials and Methods. Strains used are shown in Tables S1 and S2. The 95% confidence intervals are in parentheses.
[c] *msh6Δ* strains transformed with the empty vector pRS416.
[d] *msh6Δ* strains transformed with pSP6 encoding *msh6 K232E K271E R289E*.
[e] *msh6Δ* strains transformed with pSP3 encoding *msh6Δ290–299*.
[f] *msh6Δ* strains transformed with pSP5 encoding *msh6Δ269–299*.
[g] *msh6Δ* strains transformed with pSP4 encoding *msh6Δ252–299*.

Unlike the deletion alleles of *msh6* described above, the *msh6 R232E K271E R289E* allele conferred no phenotype in the canavanine assay (Table 3), although it was shown to cause a small but significant increase in mutation rate in the more sensitive lysine reversion assay.[40] However, when this allele was combined with *msh2Δ1*, we observed a significant (~4-fold) increase in mutation rate. As with the alleles described above, this does not appear to simply be a result of the defect in Msh2–Msh3 function. In the presence of this allele, there was a synergistic effect on mutation rate when the *msh2Δ1* and *msh3Δ* alleles were combined. Together, these data indicate that *msh2Δ1* leads to a defect in Msh2–Msh6 activity as well as a defect in Msh2–Msh3 activity. However, in the Msh2–Msh6 context, regions within the Msh6 NTR appear to compensate for the loss of Msh2 domain I.

As expected, in *msh6Δ*, there was a 9-fold increase in mutation rate over the wild type. There was a further increase in the *msh6Δ msh3Δ* background, up to about 16-fold over wild type. This is consistent with what has been observed previously when both partners for Msh2 have been eliminated.[33] Unexpectedly, there was an additional synergistic increase in mutation rate in the presence of the *msh2Δ1* allele (32-fold), suggesting that the msh2Δ1 protein may interfere with MMR-independent repair in a way that Msh2 does not.

Msh2–Msh6 and msh2Δ1–Msh6 protein complexes are present in the cell at similar levels

We considered the possibility that differences in protein levels might account for the lack of an *in vivo* phenotype in the *msh2Δ1* strain background. To address this, we examined the amount of wild-type Msh2–Msh6 and msh2Δ1–Msh6 present in the cell. We first performed quantitative Western blots of Msh2, msh2Δ1 and Msh6 (Fig. 2 and Materials and Methods; data not shown) using whole-cell lysates from wild-type, *msh2Δ* and *msh6Δ* strains (FY23, EAY281 and EAY337, respectively). We determined that there are 1600 ± 250 [standard error of the mean (SEM)] molecules of Msh2 and 1300 ± 390 (SEM) molecules of Msh6 per cell in mid-log vegetative cultures and found similar levels of msh2Δ1 and Msh2 produced under these conditions. Therefore, the deletion of Msh2 domain I does not appear to affect the levels of Msh2 in the cell. Also, the fact that we were able to purify msh2Δ1–Msh6 using the same purification protocol as Msh2–Msh6 indicates that the deletion does not grossly affect protein stability.

Based on these results, the cellular concentration of Msh2, assuming a cell volume of approximately 40 fl,[41–43] is roughly 4 μM. The local concentration within the nucleus could be up to about an order of magnitude higher, given a volume of approximately 3 fl,[41] depending on the localization of these proteins. Similarly, the cellular concentration of Msh6 is approximately 3.25 μM. This value is about five times lower than the levels measured previously[44] and is consistent with the bulk of Msh2 being in complex with Msh6.[45,46] These concentrations are well above the K_d for Msh2–Msh6 and msh2Δ1–Msh6 DNA binding (see below).

msh2Δ1–Msh6 shows defects in DNA binding specificity

The genetic analysis of *msh2Δ1* described above suggests that msh2Δ1–Msh6 defects could be compensated for by other DNA repair factors. A prediction of this analysis is that msh2Δ1–Msh6 would show defects in function when examined in isolation. msh2Δ1–Msh6 was purified using the same protocol as that for Msh2–Msh6. We investigated the DNA-binding activity of msh2Δ1–Msh6 in a gel mobility shift assay by comparing binding to a 49-mer homoduplex substrate with binding to a 49-mer substrate containing an extrahelical A nucleotide in the middle of the top strand (Fig. 3). These experiments revealed that *msh2Δ1* does confer a significant defect in Msh2–Msh6 binding activity. In particular, the mutant protein has a reduced affinity for DNA and shows no apparent preference for mispaired DNA. msh2Δ1–Msh6 binds equally well to a homoduplex and a +1 mispair DNA substrate in this assay (approximate K_d of 60 nM for each). This is in contrast to the wild-type protein, which binds mispaired substrates with higher affinity than homoduplex substrates (approximate K_d of 15 nM and 60 nM, respectively) (Fig. 3).[47–51] Furthermore, msh2Δ1–Msh6 binding to both substrates more closely resembles Msh2–Msh6 bound to the nonspecific (homoduplex) DNA substrate. Salt concentration affected the affinity but not the specificity of msh2Δ1–Msh6. Gel mobility shift experiments performed at 50 mM NaCl revealed a roughly 2-fold higher affinity of

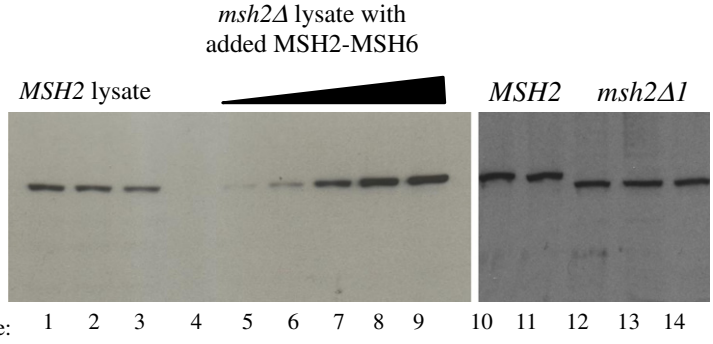

Fig. 2. Quantitative and comparative Western blots for Msh2 and msh2Δ1 using polyclonal anti-Msh2 antibody. The representative Western blots of Msh2 are shown. Lanes 1–3: three independent *MSH2* lysates from mid-log phase cultures; lanes 4–9: *msh2Δ* lysates +0, 0.26 ng, 0.52 ng, 1.04 ng, 1.56 ng and 2.08 ng of purified Msh2–Msh6, respectively. Lanes 10 and 11: *MSH2* lysate from independent mid-log phase cultures (FY23); lanes 12–14: *msh2Δ1* lysates from independent mid-log phase cultures (lanes 12 and 13, EAY2039; lane 14, EAY2040).

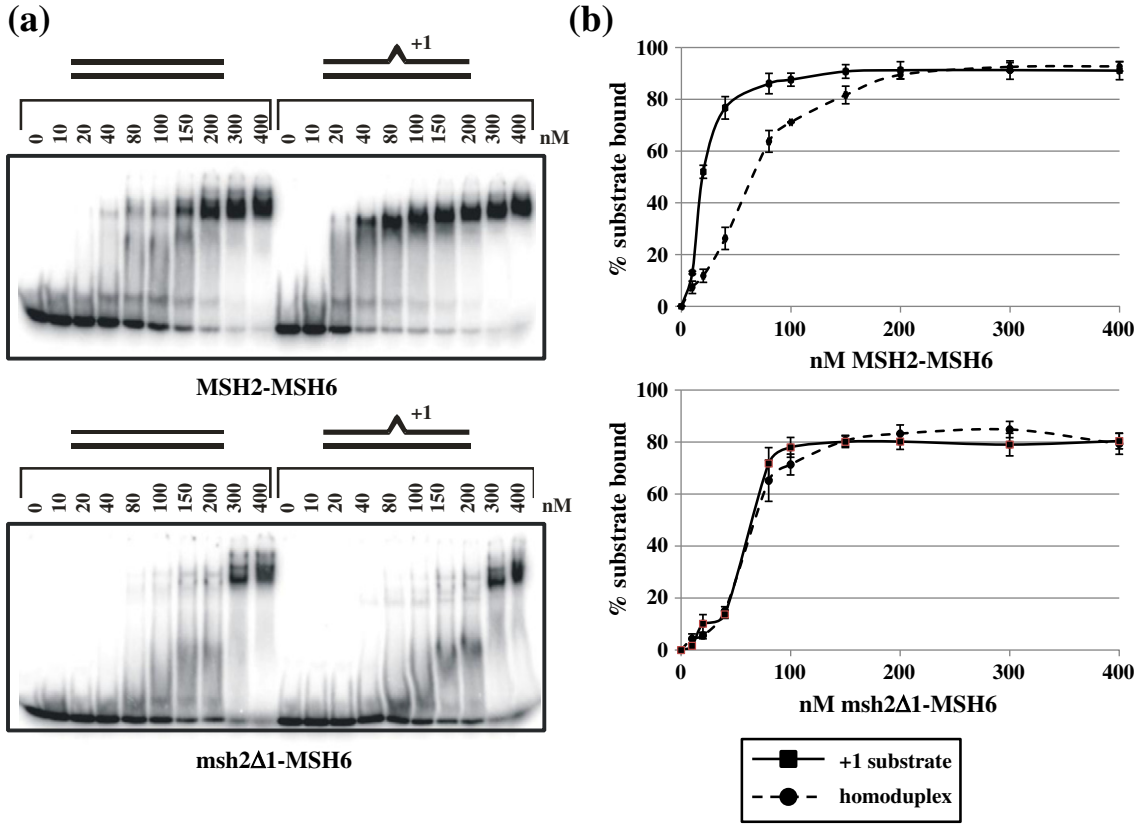

Fig. 3. Gel mobility shift assays of Msh2–Msh6 and msh2Δ1–Msh6. (a) Titration of Msh2–Msh6 (top) and msh2Δ1–Msh6 (bottom) incubated with homoduplex and +1 substrates, as described in Materials and Methods. (b) Quantification of gel mobility shift experiments showing the average binding of Msh2–Msh6 (top) and msh2Δ1–Msh6 (bottom) to a homoduplex or a +1 substrate. The error bars indicate the SEM for four (Msh2–Msh6) or five (msh2Δ1–Msh6) independent experiments.

msh2Δ1–Msh6 for both homoduplex and the +1 insertion DNA substrates; at 150 mM NaCl, the affinities decreased by about 50% for both substrates (data not shown). These data support a general reduction in affinity of msh2Δ1–Msh6 for the specific (+1 insertion) DNA substrate.

Previously, we found that msh2Δ1–Msh3 was defective in nonspecific DNA-binding activity but nonetheless retained specificity and the signature OP-Cu footprint of the wild-type protein.[28] To determine if msh2Δ1–Msh6 retained an Msh2–Msh6 signature footprint, we performed OP-Cu footprinting with Msh2–Msh6 and msh2Δ1–Msh6 using the same +1 substrate used in the gel mobility shift assay described above (Fig. 4). OP-Cu is a small chemical nuclease that cleaves in the minor groove of DNA. We performed gel mobility shift assays and treated the entire gel with OP-Cu (see Materials and Methods), excised the shifted complexes, eluted the DNA and separated the resulting fragments on a sequencing gel. The footprint is subtle, and the quantification is shown with the cleavage in the shifted complex at each position relative to the unshifted (i.e., unbound) substrate (Fig. 4a). When the DNA is protected from cleavage, the bars of the histogram are below 1.0; enhanced cleavage results in bars above 1.0. Msh2–Msh6 exhibited a discrete region (or valley) of protection on either side of the +1 nucleotide. On the top strand, about three nucleotides were protected on the 5′ side of +1, and about six nucleotides were protected on the 3′ side in the presence of Msh2–Msh6. The extrahelical nucleotide was also protected. On the bottom strand, seven nucleotides on the 5′ side and nine nucleotides on the 3′ side of +1 were protected upon Msh2–Msh6 binding (Fig. 4). This is a tighter footprint than has been observed previously using DNase I footprinting (Fig. 5)[47,52,53] and single-molecule DNA unzipping[54] (although the latter indicated a smaller footprint than the former) but is consistent with the crystal structure of human Msh2–Msh6.[10] Because OP-Cu is a small chemical, it likely has greater access to DNA in the Msh2–Msh6 nucleoprotein complex than the much larger DNase I protein. Interestingly, there is a region of enhanced cleavage about nine nucleotides

5′ of the insertion, which could be due to alterations in the DNA structure itself.

In contrast to Msh2–Msh6, msh2Δ1–Msh6 binding resulted in more extensive protection of the top strand, particularly on the 3′ side of the +1 nucleotide (Fig. 4). The extra nucleotide itself was not as strongly protected from cleavage, and there was weak protection of four nucleotides, starting approximately three nucleotides 5′ to +1. Protection of the top and bottom strands by msh2Δ1–Msh6

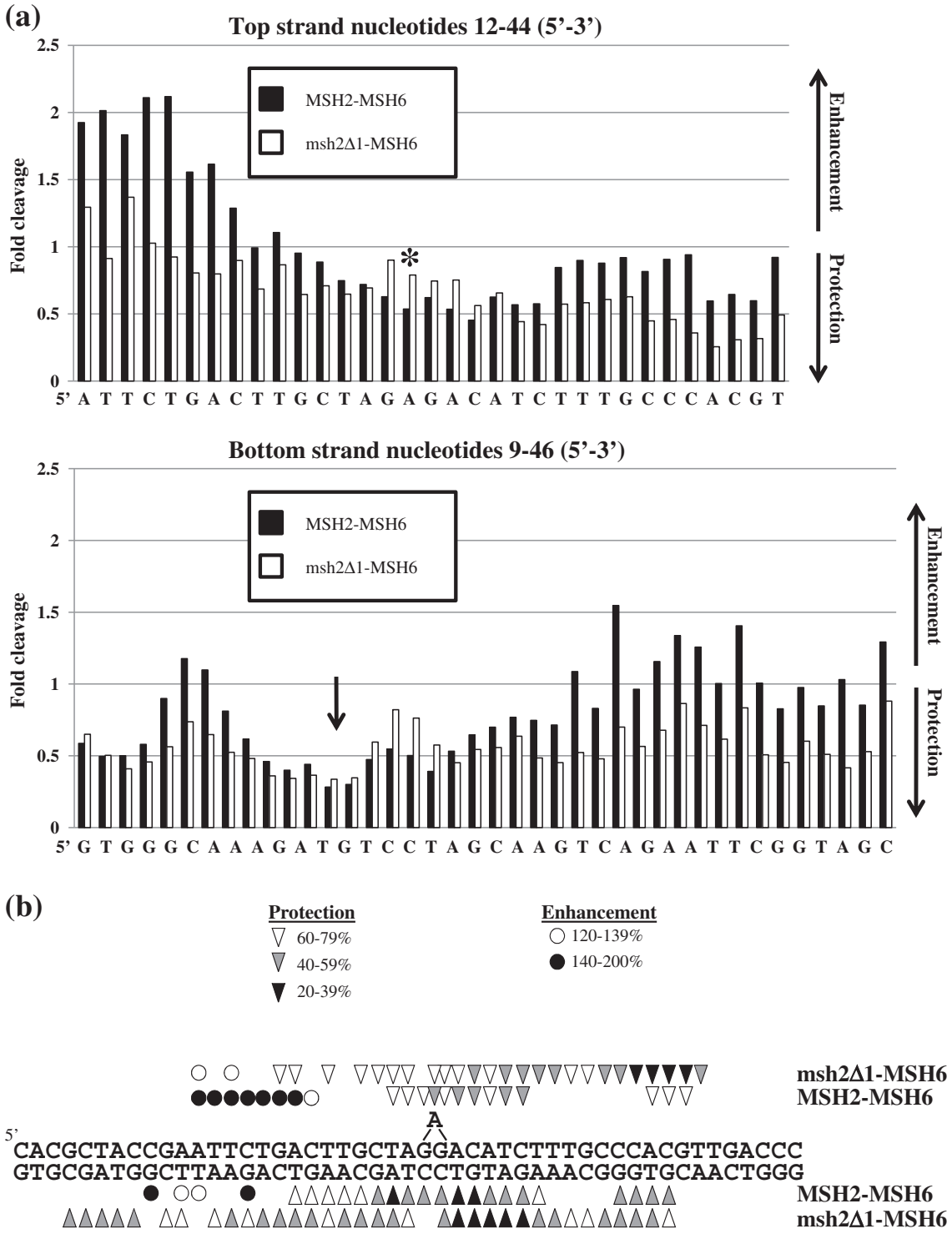

Fig. 4 (*legend on next page*)

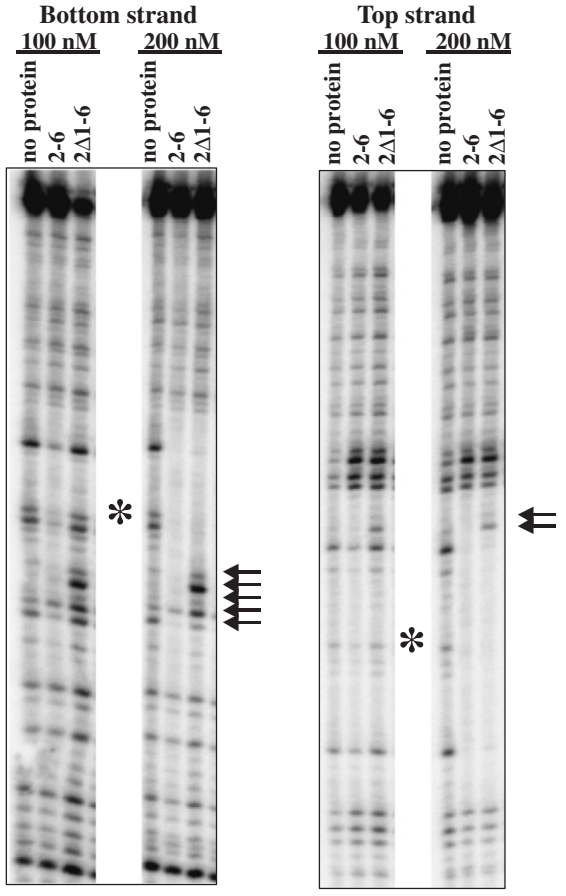

Fig. 5. DNase I protection upon binding of Msh2–Msh6 or msh2Δ1–Msh6 to a 99-mer substrate with a single +T insertion in the middle. The proteins were incubated with the DNA substrate and then treated with DNase I, as described in Materials and Methods. The left panel shows the protection pattern on the lower strand of the substrate (opposite the insertion). The right panel shows the pattern of protection on the top strand of the substrate. The arrows indicate regions of the footprint that are different in the msh2Δ1–Msh6 footprint compared to that of Msh2–Msh6. The asterisk indicates the position of the +1 extrahelical nucleotide.

was quite broad, extending at least 14 nucleotides downstream of +1 and 12 nucleotides upstream. In contrast to the pattern of protection with the wild-type protein, the residues opposite the +1 loop, on the bottom strand, were only weakly protected by msh2Δ1–Msh6 binding. These results indicate that msh2Δ1–Msh6 binds the +1 DNA substrate with less specificity than does Msh2–Msh6, resulting in an extended footprint in the presence of OP-Cu. The physical absence of Msh2 domain I may also allow access to regions of the DNA that would otherwise be occluded, such as the +1 mispair itself. It is worth noting that OP-Cu is sensitive to distortions in the DNA, and this might also affect the pattern of protection observed with msh2Δ1–Msh6.

We also compared the DNase I footprints of Msh2–Msh6 and msh2Δ1–Msh6 (Fig. 5). The footprint generated in the presence of Msh2–Msh6 was essentially the same, on both the top and the bottom strands, as previously described.[47,53] The boundaries of the DNase I footprint in the presence of msh2Δ1–Msh6 were similar to those in the presence of Msh2–Msh6. However, there were some key differences. First, a higher concentration of msh2Δ1–Msh6 was required to detect a footprint, consistent with a lower affinity for the DNA substrate. Second, binding of msh2Δ1–Msh6 led to several bands with enhanced cleavage within the footprint. These bands appeared at the lower msh2Δ1–Msh6 concentration before other portions of the footprint were protected. It is possible that the absence of Msh2 domain I allows DNase I access to this region of the DNA. Thus, while Msh2 domain I does not make direct contact with the DNA in general, it may block access to the DNA substrate. Alternatively, the mode of binding may be affected in the absence of this domain.

These footprinting data (OP-Cu and DNase I) indicate that msh2Δ1–Msh6 binds in the vicinity of the mispair but that the protection patterns differ somewhat from those of Msh2–Msh6. These differences may account for the altered specificity and affinity of msh2Δ1–Msh6 for DNA substrates. The OP-Cu and DNase I footprinting experiments provide complementary information about msh2Δ1–Msh6 binding. For instance, the relatively weak but extensive protection of the bottom strand in the presence of OP-Cu indicates reduced specificity in this region. In contrast, the DNase I footprinting indicates no apparent increase in protection of the bottom strand. Instead, five

Fig. 4. *In situ* footprinting of DNA–protein complexes with OP-Cu. Msh2–Msh6–DNA complexes or msh2Δ1–Msh6–DNA complexes were separated by gel electrophoresis and treated with OP-Cu as described in Materials and Methods. (a) Histograms of representative protection patterns of the +1 loop bottom strand substrate. Only the central portion of each substrate is shown. The signal of each band of bound DNA was normalized to the equivalent band produced in the absence of protein. Values greater than 1.0 represent enhanced cleavage; values lower than 1.0 represent protection from cleavage. The asterisk in the top panel indicates the position of the +1 nucleotide (+A). The arrow on the bottom panel indicates the position of the +A nucleotide, which is on the opposite strand. (b) Summary of OP-Cu cleavage of top and bottom strands of the +1 loop substrate in the presence of Msh2–Msh6 or msh2Δ1–Msh6 based on at least three independent experiments. Bands that were protected from cleavage are indicated by arrowheads. Enhanced cleavage is indicated by circles. The extent of enhanced cleavage or protection is indicated by the shading.

positions were cleaved more efficiently (Fig. 5, left). Interestingly, this region was strongly protected in the OP-Cu footprinting. Because OP-Cu is sensitive to DNA conformation, unlike DNase I, this may reflect a widening of the minor groove in this region to prevent OP-Cu activity. Nonetheless, these results show a clear difference between Msh2–Msh6 and msh2Δ1–Msh6 DNA binding.

msh2Δ1–Msh6 bends DNA substrates

The crystal structures of MutS homologs indicated that the DNA substrate is bent by 40–60° upon protein binding. Domain I of MutS appears to be involved in this bend,[21,22] whereas domain I of human Msh2 does not.[10] A circular permutation bending assay was developed to observe DNA bending in a gel mobility shift assay.[47,55] In this assay, a +1 IDL was placed in the middle or at either end of a 99-mer oligonucleotide substrate. When Msh2–Msh6 is bound to the +1 loop in the middle of the substrate, the mobility of the complex is slower than when the complex is formed at either end of the substrate, indicating that the DNA substrate is bent upon binding.[47] We used this assay to determine whether domain I of Msh2 is required for inducing a bend in the DNA (Fig. 6). Despite the loss in specificity and affinity of msh2Δ1–Msh6 DNA-binding activity, we found that the protein was still able to bend DNA in this assay and that the bending pattern looked like that with Msh2–Msh6.[47] Therefore, Msh2 domain I does not appear to be required to induce the bend in the DNA. This is consistent with the crystal structure of human Msh2–Msh6 in complex with a +1 substrate in which domain I of Msh2 does not make direct contact with the DNA.[10] The fact that msh2Δ1–Msh6 induces a bend in the DNA like Msh2–Msh6 indicates that it retains some specificity for the +1 loop despite the decreased affinity and specificity described above.

Discussion

Msh2 domain I is required for wild-type Msh2–Msh6 DNA-binding activity

Domain I of Msh2 plays distinct roles in Msh2–Msh6 *versus* Msh2–Msh3 *in vivo*, with this domain being largely dispensable for Msh2–Msh6 activity.[28–30] The current study provides additional evidence that Msh2 domain I has different functions in the two Msh complexes.

The crystal structure of human MutSα (Msh2–Msh6) provided mechanistic support for the lack of an Msh2–Msh6-specific phenotype in *msh2Δ1*. As had been predicted, Msh2 is the non-mismatch binding subunit.[10,24,25,27–29] However, unlike the non-mismatch binding subunit in prokaryotic MutS structures, which has extensive interactions with the DNA backbone,[21,22] domain I of Msh2 makes only one contact with the DNA backbone, through Lys6, and is predominantly rotated away from the DNA.[10] This is consistent with Msh2 domain I being dispensable for *in vivo* function of Msh2–Msh6 in *S. cerevisiae*[28] and predicts that removal of Msh2 domain I would not have a severe impact on DNA-binding activity. However, our DNA-binding data indicate that the removal of Msh2 domain I results in a severe impairment of

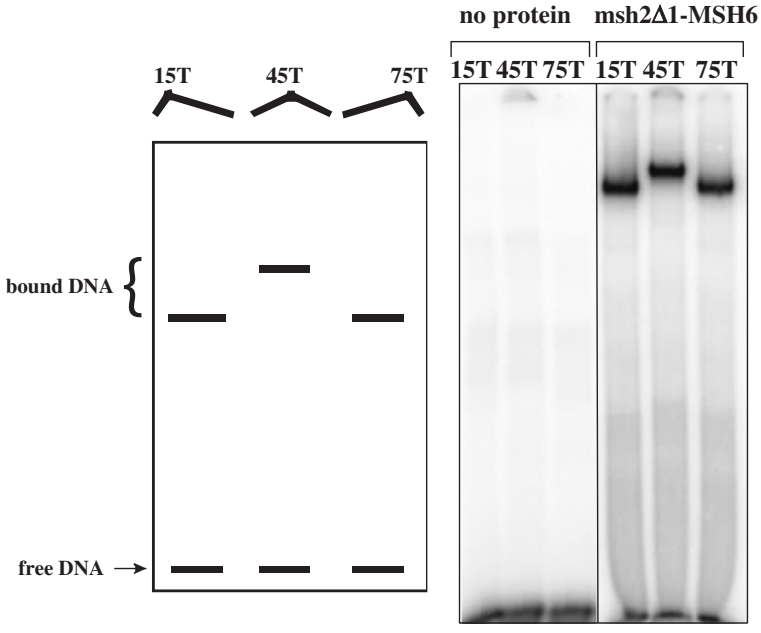

Fig. 6. DNA bending assay of msh2Δ1–Msh6. The left panel is a cartoon of the results expected if protein binding led to DNA bending. The right panel shows the unbound substrates and msh2Δ1–Msh6 (100 nM) bound to 90-mer substrates with +1 insertions at positions 15, 45 and 75, as described in Materials and Methods.

both efficiency and specificity of DNA-binding activity. Furthermore, the footprint of msh2Δ1–Msh6 on DNA by OP-Cu (Fig. 4) or DNase I (Fig. 5) is altered, indicating increased nonspecific interactions. These changes are in contrast to what we previously observed with msh2Δ1–Msh3 DNA-binding activity.[28] msh2Δ1–Msh3 had significantly reduced DNA-binding activity, but the remaining activity appeared to be specific.[28] Therefore, Msh2 domain I is important for both specific and nonspecific DNA binding in the context of Msh2–Msh6, whereas it is critical for only nonspecific binding in the context of Msh2–Msh3 bound to an IDL.

Based on the MutSα crystal structure, Msh2 domain I is not predicted to be involved in inducing the ~45° bend in the DNA.[10] Interactions between Msh6 and the DNA appear to be sufficient to generate this bend. This is in contrast to the crystal structure of *Taq* MutS, in which domain I of the nonmismatch binding subunit is hypothesized to contribute to DNA bending.[22] Our bending assay with msh2Δ1–Msh6 is consistent with the prediction based on the MutSα structure; the mutant complex retains its ability to bend a +1 mispaired substrate. Therefore, Msh2 domain I is not required for DNA bending (Fig. 6).

Low mutation rates buffer the reduced activity of msh2Δ1–Msh6 *in vivo*

Increasing the mutational load in the cell, by introducing *rad27* or *pol3* mutations, revealed defects in msh2Δ1–Msh6 activity *in vivo* (Table 1). The increase in mutations appears to saturate MMR function in the *msh2Δ1* background. This indicates that, under normal conditions, msh2Δ1–Msh6 is sufficiently active to repair the few mutations that arise, negating the biochemical defects that we observed *in vitro*. However, if is the system is stressed, the weakened msh2Δ1–Msh6 cannot function adequately.

It is worth noting that, unlike *msh2Δ*, the *msh2Δ1* allele is not synthetically lethal with *pol3-01*.[37] The *pol3-01* mutation leads to activation of the S-phase checkpoint,[56] inducing both error-prone and error-free DNA repairs, which could lead to an accumulation of mutations.[56] Datta *et al*. suggested that the synthetic lethality between *pol3-01* and *msh2Δ* is due, at least in part, to the role of Msh2 as a DNA damage sensor to activate the checkpoint.[56] If this is the case, this would suggest that *msh2Δ1* retains this function.

Msh6 NTR buffers the effect of the deletion of Msh2 domain I

The NTR of Msh6 consists of the ~300 N-terminal amino acid residues of Msh6. The crystal structure of human MutSα does not include this region,[10] and its function is not well understood. The Msh6 NTR contains the PIP box at the extreme N-terminus of the protein,[38,39] an acidic region that encodes a putative DNA mimic[40] and a nonspecific DNA-binding activity within residues 228–299.[40] We tested the ability of the PIP box and the nonspecific DNA-binding activity to buffer the deletion of Msh2 domain I in Msh2–Msh6-specific MMR activity. Both regions had an effect, but to different extents.

Disruption of the PIP box in Msh6 significantly reduces interactions with PCNA.[38,39,57] *In vivo*, these mutations resulted in small but reproducible increases in the mutation rates (Table 1), similar to previous observations.[38,39] Interestingly, the *msh2Δ1 msh3Δ msh6KQFF→AAAA* strain exhibited a significant increase in mutation rate compared to *msh3Δ msh6KQFF→AAAA* or *msh2Δ1 msh6KQFF→AAAA*, indicating that the PIP box plays a role in Msh2–Msh6 function that compensates for the loss of Msh2 domain I. These data further suggest that the effect of *msh2Δ1* is not simply due to a defect in Msh2–Msh3 activity. One possibility is that the interaction with PCNA serves to keep msh2Δ1–Msh6 in proximity to the DNA, stabilizing the bound complex on the DNA and increasing the local concentration at or near the replisome.

When we combined *msh2Δ1* with *msh6* mutations within the nonspecific DNA binding motif of the Msh6 NTR, we observed a significant effect on mutation rates, with much higher rates than those observed with the single mutants. This region of the Msh6 NTR may partially compensate for loss of nonspecific DNA-binding activity in the msh2Δ1 mutant. However, the effect of the deletions on DNA binding by the Msh6 NTR does not precisely correlate with the effect on mutation rates. *msh6 R232E K271E R289E* demonstrated the most mild phenotype in the canavanine resistance assay but had a strong effect on DNA binding,[40] similar to that of *msh6Δ252-290*, which had a stronger mutator phenotype (Table 2).[40] Therefore, this region of the NTR may have additional functions that help buffer the absence of Msh2 domain I, possibly stabilizing the Msh2–Msh6 complex or the Msh2–Msh6 complex bound to DNA.

Interestingly, sequence alignments between the NTR of Msh3 and Msh6 do not indicate the presence of a similar domain in Msh3. Therefore, Msh3 may be unable to compensate for a loss in nonspecific binding in the same way as Msh6.

Msh2 domain I in HNPCC and hereditary colon cancer

Of the domain I *MSH2* polymorphisms observed in HNPCC patients, several have been found to have no effect on MMR on their own when tested in *S. cerevisiae*, while others had either weak or strong effects on MMR.[17,18] Therefore, these alleles have varying effects on Msh2 function. Several alleles that

showed either no phenotype or a weak phenotype alone exhibited a synergistic increase in mutation rate in an *msh6Δ* background, consistent with a defect on Msh2–Msh3 activity.[18] In our work, we similarly observed a synergistic effect on mutation rate when we combined *msh2Δ1* with the *msh6* NTR alleles. However, the effect was stronger than that observed in the absence of *msh3* (Table 2), indicating an effect of the deletion in addition to its role in Msh2–Msh3 activity. Instead, it appears that the *msh2Δ1* allele makes Msh2–Msh6 activity susceptible to defects in the presence of weak *msh6* alleles in the PIP box and the NTR. Martinez and Kolodner observed a similar effect with the weak *msh2E194G* allele.[18] This allele is within domain II of Msh2 but may affect the positioning of domain I.[10,18] In a screen identifying enhancer mutations, eight weak *msh6* alleles were isolated, although none was in the NTR. The authors suggested that the *msh2* allele sensitized the Msh2–Msh6 pathway to inactivation. In both the present study and in Martinez and Kolodner,[18] Msh6 itself appears to have a buffering effect when Msh2 is compromised.

Combinations of weaker alleles are likely relevant for atypical cases of hereditary colon cancer that do not fulfill the criteria for HNPCC. Martinez and Kolodner proposed a model in which an inherited weak allele in MMR could then be combined with a somatic "second hit" mutation in another MMR gene, leading to a strong MMR defect.[18] Similarly, two different alleles could be inherited from each parent, each of which is weak, and, when combined, generate a strong defect in MMR.[58,59] Studies with *MLH1* in *S. cerevisiae* indicated that genetic background is relevant when assessing a mutator phenotype *in vivo*, particularly in the case of weaker alleles.[60] Similarly, Heck *et al.* found that natural variants in the subunits of Mlh1–Pms1 in yeast led to a defect in MMR through negative epistasis.[61] Therefore, weak alleles, such as those studied in the current work, are likely important in many cases of cancer development, and it may be important to analyze multiple MMR genes in microsatellite instability positive tumors in order to identify a combination of mutations responsible for the disease phenotype.

Despite the mild mutator phenotype, domain I of Msh2 is essential for intact Msh2–Msh6 function. The ability of the cell to buffer biochemical defects in the *msh2Δ1* background is striking and should be considered when evaluating the effects of putative HNPCC mutations in *in vivo* assays.

Materials and Methods

Plasmids and yeast strain construction

All yeast transformations were performed using the lithium acetate method.[62] Yeast strains were derived from the S288c background and are detailed in Supplementary Tables 1 and 2.

To make an *msh2Δ1* allele without the hemagglutinin tag that was present in our earlier work,[28] we created an untagged version of our integration vector (pEAI169).[30] Briefly, we replaced the 3′ end of *msh2Δ1-HA*$_4$ with a BlpI-NheI fragment from the 3′ end of *MSH2* from pMMR8.[63] This generated the single-step integration vector pEAI245, which was digested with PvuI and PvuII and used to introduce *msh2Δ1::LEU2* into FY23 (*MAT*α) and FY86 (*MAT***a**),[31] as well as other strain backgrounds (Tables S1 and S2). Integrations were verified by PCR.

The *pol3-01* and *rad27* alleles were introduced into the *msh2Δ1* background by mating followed by sporulation and tetrad dissection. For *pol3-01*, EAY565 (*MAT***a** *ura3-52 leu2Δ trp1Δ63 pol3-01*)[35] was mated with EAY2039 and EAY2040 (both *MAT*α *msh2Δ1::LEU2*). For *rad27G67S*, EAY595 (*MAT***a** *leu2Δ1 ade8 rad27-G67S*) was mated with EAY2040 (*MAT*α *msh2Δ1::LEU2*). The diploids were sporulated, and four spore tetrads were replicated onto synthetic complete (SC)-leucine to select for *msh2Δ1*. For *pol3-01*, Leu$^+$ colonies were tested for the presence of the allele by PCR, followed by diagnostic digestion by BstUI and EcoRV. For *rad27-G67S*, Leu$^+$ colonies were first tested by qualitative canavanine patch assay (*rad27* alleles have high mutator activity)[64] and on 0.02% methyl methanesulfonate plates (*rad27* alleles are methyl methanesulfonate sensitive).[64]

The *msh3Δ* strains were constructed by integrative transformation with pEAI88 (*msh3Δ::hisG-URA3-hisG*) digested with EcoRI. Transformants were selected on SC-uracil. Spontaneous loss of *URA3* (pop-out) was then selected on 5-fluoroorotic acid. Integration and pop-out events were verified by PCR.

The *msh6Δ* strains were constructed by amplifying a chromosomal *msh6Δ::KANMX* fragment from the yeast deletion collection. The resulting PCR product was used to transform various yeast strains. The transformants were selected on YPD+G418, and integration was verified by PCR.

The integrative plasmid used to introduce the PCNA binding mutation into *MSH6* was obtained from the Kunkel laboratory.[38] In this plasmid, the sequence encoding the KQFF residues within the conserved PCNA binding motif was mutated to instead encode AAAA. The plasmid was digested with AflII and used to transform the appropriate strains. Transformants were selected on SC-Ura, and then, *URA3* was popped out on 5-fluoroorotic acid. The presence of the mutations was verified by PCR followed by diagnostic digests and DNA sequencing.

MSH6 and *msh6* alleles on low-copy-number plasmids were obtained from the Kunkel laboratory.[40] HindIII-BamHI fragments of these plasmids were sub-cloned into pRS416, which carries the *URA3* marker.

Mutational analyses

Quantitative canavanine resistance assays were performed as described previously.[30] For most strains, we analyzed mutation rates from at least two isolates. We calculated mutation rates for the individual isolates (at least 22 individual colonies) and found that they were statistically the same. We therefore grouped the data from the isolates in each strain to generate the mutation rates shown in Tables 1 and 2. When a single isolate was tested,

at least 44 individual colonies were used to calculate mutation rates. We used the Ma–Sandri–Sarkar Maximum Likelihood Estimator method[65] to calculate mutation rates and 95% confidence intervals. We developed a spreadsheet to facilitate these calculations. Subsequently, Hall *et al.* developed a web tool for these calculations (FALCOR),[66] which we used to validate our calculations.

The *m* values calculated by the Ma–Sandri–Sarkar Maximum Likelihood Estimator are normally distributed. Therefore, we carried out student *t*-tests between pairs to determine *p* values. Differences were considered significant when $p<0.01$.

For the mutation spectra, canavanine-resistant papillations from wild-type and *msh2Δ1* strains were selected. The *CAN1* gene was amplified by PCR and analyzed by DNA sequencing.

Msh2–Msh6 and msh2Δ1–Msh6 purifications

For overexpression and purification of msh2Δ1, we digested pEAE9[67] with NheI and XhoI and replaced it with an *msh2Δ1* fragment amplified from pEAI169[30] to generate pEAE263. We then inserted the BglII fragment from YEp13, which encodes the *LEU2* marker, into the BglII site of pEAE263 to generate pEAE248.

Msh2–Msh6 was overexpressed and purified from a protease-deficient strain of *S. cerevisiae* (EAY33) containing pEAE9 (*MSH2*) and pEAE219 (*MSH6*) as described previously.[47] msh2Δ1–Msh6 was purified using pEAE248 (*msh2Δ1*) and pEAE219. msh2Δ1–Msh6 was purified from EAY158, a protease-deficient yeast derivative of EAY33 deleted for *MSH2*. msh2Δ1–Msh6 purified with yields similar to those of wild type, suggesting that the deletion mutation did not disrupt protein stability. Protein concentrations were determined in the Bradford assay using bovine serum albumin (Sigma-Aldrich) as a standard.

Gel mobility shift assays

The 49-mer DNA substrates used in gel mobility shift assays were homoduplex (LS1/LS2) and +1 insertion (LS2/LS6), as described previously.[68] The extrahelical nucleotide is A. Substrates were prepared as described previously.[68] The standard DNA binding assay (10 μl) contained 50 nM 5′ end-labeled [^{32}P]substrate in 20 mM Hepes (pH 7.5), 100 mM NaCl, 1 mM DTT and 40 μg/ml of bovine serum albumin. Reactions were assembled on ice with Msh2–Msh6 or msh2Δ1–Msh6 added last and then incubated at room temperature for 5 min. Samples were electrophoresed through 4% non-denaturing polyacrylamide (29:1) gels in 45 mM Tris–borate and 0.5 mM ethylenediaminetetraacetic acid (EDTA) (pH 8.0) at 130 V for 45 min in a water-cooled gel electrophoresis apparatus. Gels were dried and exposed to a PhosphorImager screen (Molecular Dynamics) and quantified with ImageQuant (Amersham). The percent of bound substrate consisted of all substrates shifted above the unbound DNA substrate. Approximate K_d was defined as the protein concentration at which 50% of the DNA substrate was bound.

In situ OP-Cu footprinting

In situ OP-Cu footprinting was performed as described,[68] using the same substrates as in the gel mobility shift assays. Briefly, binding reactions were performed in 10-μl volumes containing 1–2 pmol ^{32}P-labeled DNA substrate as described above for the gel mobility shift assays. Sonicated salmon sperm DNA (100 ng) was added to each reaction. Protein–DNA complexes were separated by electrophoresis through a 6% non-denaturing polyacrylamide gel. The gel was immersed in 10 mM Tris–HCl (pH 8.0) and then treated with 20 ml of solution A (2 mM OP-Cu and 0.45 mM $CuSO_4$; Sigma-Aldrich) and 20 ml of solution B (1:200 dilution of 3-mercaptopropionic acid in ddH_20; Sigma-Aldrich). After 15 min at room temperature, digestion was stopped by the addition of 20 ml of solution C (28 mM neocuproine; Sigma-Aldrich). Protein–DNA complexes and free DNA bands were located by autoradiography of the wet gel and excised, crushed and eluted overnight at 37 °C in 0.5 M ammonium acetate and 1 mM EDTA (pH 8.0). The extracted DNA was phenol: chloroform extracted, precipitated with ethanol, dried and resuspended in 6 μl of loading dye [98% formamide, 10 mM EDTA (pH 8.0), 0.025% xylene cyanol and 0.025% bromophenol blue]. Samples were separated by electrophoresis on 10% denaturing urea polyacrylamide gels. Sequencing standards were created by dimethyl sulfate (Sigma-Aldrich) modification of DNA substrates and cleavage with NaOH to generate G→A DNA ladders. The gels were dried on DE81 paper and exposed to a PhosphorImager screen for quantification (ImageQuant). The footprint patterns were quantified by normalizing each band relative to the total counts per lane.

DNase I footprinting

DNase I footprinting was performed essentially as previously described.[47] Briefly, Msh2–Msh6–DNA complexes were formed at room temperature in a 25-μl reaction containing either a radiolabeled 99-mer substrate with a +T insertion in the center of the substrate (+1 substrate) or a 99-mer homoduplex DNA substrate.[47] DNase I (0.33 units; New England Biolabs) was added to each reaction and incubated for 2 min at room temperature. Stop buffer (90 μl) (1.6 M ammonium acetate, 400 μg/ml of sonicated salmon sperm DNA and 0.1 mM EDTA) was added to quench the reaction. The samples were phenol:chloroform extracted twice, chloroform extracted and then precipitated with ethanol. The pellets were air dried and resuspended in 6 μl of formamide dye.[69] The reactions were electrophoresed through a 10% acrylamide, 50% urea and 1× Tris–borate–EDTA sequencing gel at 75 W for 90 min. The DNase I reactions were run alongside dimethyl-sulfate-modified sequencing reactions of the same substrates, which were included as markers. Gels were dried onto DE81 paper and exposed to a PhosphorImager screen. The data were visualized and analyzed by ImageQuant.

DNA bending assay

DNA bending assays were performed essentially as previously described.[47,55] Briefly, duplex 90-base-pair DNA substrates containing a single T insertion at positions 15, 45 and 75 were radiolabeled and used as substrates in a gel mobility shift assay with Msh2–Msh6 or msh2Δ1–Msh6. Approximately 200 ng of pBluescript was added to the reaction just prior to electrophoresis. Samples

were separated by electrophoresis in a water-cooled apparatus at 250 V for 90 min. The gels were dried on 3MM Whatman paper and exposed to a PhosphorImager screen. The data were visualized by ImageQuant.

Quantitative Western blots

The *MSH2* strain used was FY23,[31] the *msh2Δ* strain was EAY281[70] and the *msh2Δ1* strains were EAY2039 and EAY2040 (this study, Table S1). Polyclonal antibodies against *S. cerevisiae* Msh2 and Msh6 were previously described.[71]

Cultures were grown to $OD_{600} = 0.6$, and the cells were lysed as previously described.[72] Three replicates of wild type, six replicates of *msh2Δ* and *msh6Δ* and three replicates of *msh2Δ1* were performed. Dilutions of the cells just prior to lysis and just after lysis were counted on a hemacytometer (in triplicate for quantitative blots) to determine the lysis efficiency and the cell concentrations. Cell lysates or purified protein was run by SDS-PAGE and then transferred to Bio-Rad Laboratories Trans-Blot nitrocellulose (Hercules, CA) by full immersion in a Mini Trans-Blot Cell (Bio-Rad). The membrane was blocked overnight at 4 °C and then incubated with the 1:4000 diluted primary anti-Msh2 or anti-Msh6 antibody for 1 h, followed by incubation with 1:4000 diluted horseradish-peroxidase-conjugated goat anti-rabbit antibody for 1 h. It was then treated for chemiluminescent detection as directed with the Amersham ECL Plus System (GE Healthcare). The membrane was exposed to Kodak BioMax Light film.

For quantitative blots, equal-volume replicates from the same aliquot of wild-type cell lysate that were calculated to contain 2.3×10^6 lysed cells were loaded to monitor consistency. This number of lysed cells provided amounts of Msh2 or Msh6 that were in the linear range for measurement. For a standard curve, increasing amounts of purified Msh2–Msh6 heterodimer were added back to null strain lysate, which controlled for possible cross-reacting proteins.

For comparative blots, one or more lanes of wild-type cell lysate were loaded to provide a reference. An equal number of lysed cells for each strain were loaded.

Developed film images were scanned into Tiff files at 300 dpi and processed with Adobe Photoshop CS2, Version 9.0.2. One box fitting the largest band on the gel was used to take the measurements (mean gray value) of each band and of the background of every lane directly below the desired band. Background values were subtracted from band values to give the band intensity.

The band intensity was plotted over the number of Msh2 or Msh6 molecules/cell loaded. To calculate the lysate volume needed to load 2.3×10^6 lysed cells (cell equivalents), we calculated the concentration of cell equivalents in the lysate: the mean of the three post-lysis cell counts was divided by the mean of the three pre-lysis cell counts, and the resulting value was subtracted from 1.00 to give the lysis efficiency. The lysis efficiency was multiplied by the pre-lysis cell concentration to give the concentration of cell equivalents in the lysate. In the reference standard lanes, the same calculation was performed with the null strain lysate to load 2.3×10^6 lysed cells, and then zero, 0.26 ng, 0.53 ng, 1.04 ng, 1.56 ng or 2.08 ng of Msh2–Msh6 dimer was added to the null strain lysate to make the standard curve. A linear regression line was then fit to the curve with MS Office Excel 2003, and the equation was used to solve for the number of Msh2 or Msh6 molecules/cell in each wild-type lane. Three quantitative blots were made for both Msh2 and Msh6 using independent cultures, and SEM is the SEM for the three independent experiments.

Supplementary materials related to this article can be found online at doi:10.1016/j.jmb.2011.06.030

Acknowledgements

We thank Dr. Tom Kunkel for providing us with the *msh6* allele plasmids. We thank Dr. Susan Lee and Dr. Elaine Sia for discussions regarding this work. We thank Dr. Mark Sutton and members of the Surtees laboratory, especially Dr. Eugen Minca, for their critical reading of the manuscript. C.K., S.P., A.R.B., J.O. and J.A.S. were supported by National Institutes of Health GM087459. E.A. and J.S. were supported by National Institutes of Health GM53085.

References

1. Kunkel, T. A. & Erie, D. A. (2005). DNA mismatch repair. *Annu. Rev. Biochem.* **74**, 681–710.
2. Jiricny, J. (2006). The multifaceted mismatch-repair system. *Nat. Rev., Mol. Cell Biol.* **7**, 335–346.
3. Li, G. M. (2008). Mechanisms and functions of DNA mismatch repair. *Cell Res.* **18**, 85–98.
4. Modrich, P. & Lahue, R. (1996). Mismatch repair in replication fidelity, genetic recombination, and cancer biology. *Annu. Rev. Biochem.* **65**, 101–133.
5. Peltomaki, P. (2005). Lynch syndrome genes. *Fam. Cancer*, **4**, 227–232.
6. Heinen, C. D. (2010). Genotype to phenotype: analyzing the effects of inherited mutations in colorectal cancer families. *Mutat. Res.* **693**, 32–45.
7. Duraturo, F., Liccardo, R., Cavallo, A., Rosa, M. D., Grosso, M. & Izzo, P. (2010). Association of low-risk *MSH3* and *MSH2* variant alleles with Lynch syndrome: probability of synergistic effects.*Int. J. Cancer,* [Epub ahead of print].
8. Jensen, L. E., Jauert, P. A. & Kirkpatrick, D. T. (2005). The large loop repair and mismatch repair pathways of *Saccharomyces cerevisiae* act on distinct substrates during meiosis. *Genetics*, **170**, 1033–1043.
9. Harrington, J. M. & Kolodner, R. D. (2007). *Saccharomyces cerevisiae* Msh2–Msh3 acts in repair of base–base mispairs. *Mol. Cell. Biol.* **27**, 6546–6554.
10. Warren, J. J., Pohlhaus, T. J., Changela, A., Iyer, R. R., Modrich, P. L. & Beese, L. S. (2007). Structure of the human MutSα DNA lesion recognition complex. *Mol. Cell*, **26**, 579–592.
11. Peltomaki, P. (2003). Role of DNA mismatch repair defects in the pathogenesis of human cancer. *J. Clin. Oncol.* **21**, 1174–1179.
12. Stenson, P. D., Ball, E. V., Mort, M., Phillips, A. D., Shiel, J. A., Thomas, N. S. T. *et al.* (2003). Human gene

mutation database (HGMD®): 2003 update. *Hum. Mutat.* **21**, 577–581.
13. Chao, E. C., Velasquez, J. L., Witherspoon, M. S. L., Rozek, L. S., Peel, D., Ng, P. *et al.* (2008). Accurate classification of *MLH1/MSH2* missense variants with multivariate analysis of protein polymorphisms–mismatch repair (MAPP-MMR). *Hum. Mutat.* **29**, 852–860.
14. Lastella, P., Surdo, N., Resta, N., Guanti, G. & Stella, A. (2006). In silico and *in vivo* splicing analysis of *MLH1* and *MSH2* missense mutations shows exon- and tissue-specific effects. *BMC Genomics*, **7**, 243.
15. Ollila, S., Dermadi Bebek, D., Jiricny, J. & Nyström, M. (2008). Mechanisms of pathogenicity in human *MSH2* missense mutants. *Hum. Mutat.* **29**, 1355–1363.
16. Ollila, S., Sarantaus, L., Kariola, R., Chan, P., Hampel, H., Holinski-Feder, E. *et al.* (2006). Pathogenicity of *MSH2* missense mutations is typically associated with impaired repair capability of the mutated protein. *Gastroenterology*, **131**, 1408–1417.
17. Gammie, A. E., Erdeniz, N., Beaver, J., Devlin, B., Nanji, A. & Rose, M. D. (2007). Functional characterization of pathogenic human *MSH2* missense mutations in *Saccharomyces cerevisiae*. *Genetics*, **177**, 707–721.
18. Martinez, S. L. & Kolodner, R. D. Functional analysis of human mismatch repair gene mutations identifies weak alleles and polymorphisms capable of polygenic interactions. *Proc. Natl Acad. Sci. USA* **107**, 5070–5075.
19. Wang, Y., Friedl, W., Lamberti, C., Jungck, M., Mathiak, M., Pagenstecher, C. *et al.* (2003). Hereditary nonpolyposis colorectal cancer: frequent occurrence of large genomic deletions in *MSH2* and *MLH1* genes. *Int. J. Cancer*, **103**, 636–641.
20. Tournier, I., Vezain, M., Martins, A., Charbonnier, F., Baert-Desurmont, S., Olschwang, S. *et al.* (2008). A large fraction of unclassified variants of the mismatch repair genes *MLH1* and *MSH2* is associated with splicing defects. *Hum. Mutat.* **29**, 1412–1424.
21. Lamers, M. H., Perrakis, A., Enzlin, J. H., Winterwerp, H. H. K., de Wind, N. & Sixma, T. K. (2000). The crystal structure of DNA mismatch repair protein MutS binding to a G·T mismatch. *Nature*, **407**, 711–717.
22. Obmolova, G., Ban, C., Hsieh, P. & Yang, W. (2000). Crystal structures of mismatch repair protein MutS and its complex with a substrate DNA. *Nature*, **407**, 703–710.
23. Schofield, M. J., Brownewell, F. E., Nayak, S., Du, C., Kool, E. T. & Hsieh, P. (2001). The Phe-*X*-Glu DNA binding motif of MutS. *J. Biol. Chem*, **276**, 45505–45508.
24. Bowers, J., Sokolsky, T., Quach, T. & Alani, E. (1999). A mutation in the Msh6 subunit of the *Saccharomyces cerevisiae* Msh2–Msh6 complex disrupts mismatch recognition. *J. Biol. Chem.* **274**, 16115–16125.
25. Drotschmann, K., Yang, W., Brownewell, F. E., Kool, E. T. & Kunkel, T. A. (2001). Asymmetric recognition of DNA local distortion. Structure-based functional studies of eukaryotic Msh2–Msh6. *J. Biol. Chem.* **276**, 46225–46229.
26. Das Gupta, R. & Kolodner, R. D. (2000). Novel dominant mutations in *Saccharomyces cerevisiae MSH6*. *Nat. Genet*. **24**, 53–56.
27. Dufner, P., Marra, G., Raschle, M. & Jiricny, J. (2000). Mismatch recognition and DNA-dependent stimulation of the ATPase activity of hMutSα is abolished by a single mutation in the hMsh6 subunit. *J. Biol. Chem.* **275**, 36550–36555.
28. Lee, S. D., Surtees, J. A. & Alani, E. (2007). *Saccharomyces cerevisiae* Msh2–Msh3 and Msh2–Msh6 complexes display distinct requirements for DNA binding domain I in mismatch recognition. *J. Mol. Biol.* **366**, 53–66.
29. Shell, S. S., Putnam, C. D. & Kolodner, R. D. (2007). Chimeric *Saccharomyces cerevisiae* Msh6 protein with an Msh3 mispair-binding domain combines properties of both proteins. *Proc. Natl Acad. Sci. USA*, **104**, 10956–10961.
30. Goldfarb, T. & Alani, E. (2005). Distinct roles for the *Saccharomyces cerevisiae* mismatch repair proteins in heteroduplex rejection, mismatch repair and nonhomologous tail removal. *Genetics*, **169**, 563–574.
31. Winston, F., Dollard, C. & SL, R. H. (1995). Construction of a set of convenient *Saccharomyces cerevisiae* strains that are isogenic to S288c. *Yeast*, **11**, 53–55.
32. Xu, X., Page, J. L., Surtees, J. A., Liu, H., Lagedrost, S., Lu, Y. *et al.* (2008). Broad overexpression of ribonucleotide reductase genes in mice specifically induces lung neoplasms. *Cancer Res.* **68**, 2652–2660.
33. Marsischky, G. T., Filosi, N., Kane, M. F. & Kolodner, R. D. (1996). Redundancy of *Saccharomyces cerevisiae MSH3* and *MSH6* in *MSH2*-dependent mismatch repair. *Genes Dev.* **10**, 407–420.
34. Burgers, P. M. J. (2009). Polymerase dynamics at the eukaryotic DNA replication fork. *J. Biol. Chem.* **284**, 4041–4045.
35. Xie, Y., Counter, C. & Alani, E. (1999). Characterization of the repeat-tract instability and mutator phenotypes conferred by a *Tn3* insertion in *RFC1*, the large subunit of the yeast clamp loader. *Genetics*, **151**, 499–509.
36. Morrison, A., Johnson, A., Johnston, L. & Sugino, A. (1993). Pathway correcting DNA replication errors in *Saccharomyces cerevisiae*. *EMBO J.* **12**, 1467–1473.
37. Tran, H. T., Gordenin, D. A. & Resnick, M. A. (1999). The 3′→5′ exonucleases of DNA polymerases delta and epsilon and the 5′→3′ exonuclease Exo1 have major roles in postreplication mutation avoidance in *Saccharomyces cerevisiae*. *Mol. Cell. Biol.* **19**, 2000–2007.
38. Clark, A. B., Valle, F., Drotschmann, K., Gary, R. K. & Kunkel, T. A. (2000). Functional interaction of proliferating cell nuclear antigen with Msh2–Msh6 and Msh2–Msh3 complexes. *J. Biol. Chem.* **275**, 36498–36501.
39. Flores-Rozas, H., Clark, D. & Kolodner, R. D. (2000). Proliferating cell nuclear antigen and Msh2p–Msh6p interact to form an active mispair recognition complex. *Nat. Genet*. **26**, 375–378.
40. Clark, A. B., Deterding, L., Tomer, K. B. & Kunkel, T. A. (2007). Multiple functions for the N-terminal region of Msh6. *Nucleic Acids Res.* **35**, 4114–4123.
41. Jorgensen, P., Edgington, N. P., Schneider, B. L., Rupes, I., Tyers, M. & Futcher, B. (2007). The size of the nucleus increases as yeast cells grow. *Mol. Biol. Cell*, **18**, 3523–3532.
42. Tyson, C. B., Lord, P. G. & Wheals, A. E. (1979). Dependency of size of *Saccharomyces cerevisiae* cells on growth rate. *J. Bacteriol.* **138**, 92–98.
43. Jorgensen, P., Nishikawa, J. L., Breitkreutz, B. J. & Tyers, M. (2002). Systematic identification of pathways

that couple cell growth and division in yeast. *Science*, **297**, 395–400.
44. Ghaemmaghami, S., Huh, W. K., Bower, K., Howson, R. W., Belle, A., Dephoure, N. *et al.* (2003). Global analysis of protein expression in yeast. *Nature*, **425**, 737–741.
45. Marra, G., Iaccarino, I., Lettieri, T., Roscilli, G., Delmastro, P. & Jiricny, J. (1998). Mismatch repair deficiency associated with overexpression of the *MSH3* gene. *Proc. Natl Acad. Sci. USA*, **95**, 8568–8573.
46. Tian, L., Gu, L. & Li, G. M. (2009). Distinct nucleotide binding/hydrolysis properties and molar ratio of MutSα and MutSΔ determine their differential mismatch binding activities. *J. Biol. Chem.* **284**, 11557–11562.
47. Kijas, A. W., Studamire, B. & Alani, E. (2003). Msh2 separation of function mutations confer defects in the initiation steps of mismatch repair. *J. Mol. Biol.* **331**, 123–138.
48. Bowers, J., Tran, P. T., Liskay, R. M. & Alani, E. (2000). Analysis of yeast Msh2–Msh6 suggests that the initiation of mismatch repair can be separated into discrete steps. *J. Mol. Biol.* **302**, 327–338.
49. Marsischky, G. T. & Kolodner, R. D. (1999). Biochemical characterization of the interaction between the *Saccharomyces cerevisiae* Msh2–Msh6 complex and mispaired bases in DNA. *J. Biol. Chem.* **274**, 26668–26682.
50. Acharya, S., Wilson, T., Gradia, S., Kane, F., Guerrette, S., Marsischky, T. *et al.* (1996). hMSH2 forms specific mispair-binding complexes with hMSH3 and hMSH6. *Proc. Natl Acad. Sci. USA*, **93**, 13629–13634.
51. Gradia, S., Subramanian, T., Acharya, S., Makhov, A., Griffith, J. & Fishel, R. (1999). hMsh2–hMsh6 forms a hydrolysis-independent sliding clamp in mismatched DNA. *Mol. Cell*, **3**, 255–261.
52. Alani, E., Lee, J. Y., Schofield, M. J., Kijas, A. W., Hsieh, P. & Yang, W. (2003). Crystal structure and biochemical analysis of the MutS·ADP·beryllium fluoride complex suggests a conserved mechanism for ATP interactions in mismatch repair. *J. Biol. Chem.* **278**, 16088–16094.
53. Gradia, S., Acharya, S. & Fishel, R. (1997). The human mismatch recognition complex hMSH2–hMSH6 functions as a novel molecular switch. *Cell*, **91**, 995–1005.
54. Jiang, J., Bai, L., Surtees, J. A., Gemici, Z., Wang, M. D. & Alani, E. (2005). Detection of high-affinity and sliding clamp modes for Msh2–Msh6 by single-molecule unzipping force analysis. *Mol. Cell*, **20**, 771–781.
55. Wang, H., Yang, Y., Schofield, M. J., Du, C., Fridman, Y., Lee, S. D. *et al.* (2003). DNA bending and unbending by muts govern mismatch recognition and specificity. *Proc. Natl Acad. Sci. USA*, **100**, 14822–14827.
56. Datta, A., Schmeits, J. L., Amin, N. S., Lau, P. J., Myung, K. & Kolodner, R. D. (2000). Checkpoint-dependent activation of mutagenic repair in *Saccharomyces cerevisiae pol3-01* mutants. *Mol. Cell*, **6**, 593–603.
57. Lee, S. D. & Alani, E. (2006). Analysis of interactions between mismatch repair initiation factors and the replication processivity factor PCNA. *J. Mol. Biol.* **355**, 175–184.
58. Kariola, R., Otway, R., Lönnqvist, K., Raevaara, T., Macrae, F., Vos, Y. *et al.* (2003). Two mismatch repair gene mutations found in a colon cancer patient—which one is pathogenic? *Hum. Genet.* **112**, 105–109.
59. Plaschke, J., Linnebacher, M., Kloor, M., Gebert, J., Cremer, F. W., Tinschert, S. *et al.* (2006). Compound heterozygosity for two *msh6* mutations in a patient with early onset of HNPCC-associated cancers, but without hematological malignancy and brain tumor. *Eur. J. Hum. Genet.* **14**, 561–566.
60. Wanat, J. J., Singh, N. & Alani, E. (2007). The effect of genetic background on the function of *Saccharomyces cerevisiae MLH1* alleles that correspond to HNPCC missense mutations. *Hum. Mol. Genet.* **16**, 445–452.
61. Heck, J. A., Argueso, J. L., Gemici, Z., Reeves, R. G., Bernard, A., Aquadro, C. F. & Alani, E. (2006). Negative epistasis between natural variants of the *Saccharomyces cerevisiae MLH1* and *PMS1* genes results in a defect in mismatch repair. *Proc. Natl Acad. Sci. USA*, **103**, 3256–3261.
62. Gietz, D., Jean, A. S., Woods, R. A. & Schiestl, R. H. (1992). Improved method for high efficiency transformation of intact yeast cells. *Nucleic Acids Res.* **20**, 1425.
63. Habraken, Y., Sung, P., Prakash, L. & Prakash, S. (1996). Binding of insertion/deletion DNA mismatches by the heterodimer of yeast mismatch repair proteins Msh2 and Msh3. *Curr. Biol.* **6**, 1185–1187.
64. Xie, Y., Liu, Y., Argueso, J. L., Henricksen, L. A., Kao, H. I., Bambara, R. A. & Alani, E. (2001). Identification of *rad27* mutations that confer differential defects in mutation avoidance, repeat tract instability, and flap cleavage. *Mol. Cell. Biol.* **21**, 4889–4899.
65. Foster, P. L., Judith, L. C. & Paul, M. (2006). Methods for determining spontaneous mutation rates. *Methods Enzymol.* **409**, 195–213.
66. Hall, B. M., Ma, C. X., Liang, P. & Singh, K. K. (2009). Fluctuation analysis calculator: a web tool for the determination of mutation rate using Luria–Delbrück fluctuation analysis. *Bioinformatics*, **25**, 1564–1565.
67. Alani, E. (1996). The *Saccharomyces cerevisiae* Msh2 and Msh6 proteins form a complex that specifically binds to duplex oligonucleotides containing mismatched DNA base pairs. *Mol. Cell. Biol.* **16**, 5604–5615.
68. Surtees, J. A. & Alani, E. (2006). Mismatch repair factor Msh2–Msh3 binds and alters the conformation of branched DNA structures predicted to form during genetic recombination. *J. Mol. Biol.* **360**, 523–536.
69. Sambrook, J., Fritsch, E. F. & Maniatis, T. (1989). *Molecular Cloning: A Laboratory Manual*, 2nd edit. Cold Spring Harbor Press, Cold Spring Harbor, NY.
70. Studamire, B., Price, G., Sugawara, N., Haber, J. E. & Alani, E. (1999). Separation-of-function mutations in *Saccharomyces cerevisiae msh2* that confer mismatch repair defects but do not affect nonhomologous-tail removal during recombination. *Mol. Cell. Biol.* **19**, 7558–7567.
71. Studamire, B., Quach, T. & Alani, E. (1998). *Saccharomyces cerevisiae* Msh2p and Msh6p ATPase activities are both required during mismatch repair. *Mol. Cell. Biol.* **18**, 7590–7601.
72. Sokolsky, T. & Alani, E. (2000). *EXO1* and *MSH6* are high-copy suppressors of conditional mutations in the *MSH2* mismatch repair gene of *Saccharomyces cerevisiae*. *Genetics*, **155**, 589–599.